

Comments on the minimal training set for CNN: a case study of the frustrated J_1 - J_2 Ising model on the square lattice

Shang-Wei Li, Yuan-Heng Tseng, Ming-Che Hsieh, and Fu-Jiun Jiang*

Department of Physics, National Taiwan Normal University, 88, Sec.4, Ting-Chou Rd., Taipei 116, Taiwan

The minimal training set to train a working CNN is explored in detail. The considered model is the frustrated J_1 - J_2 Ising model on the square lattice. Here $J_1 < 0$ and $J_2 > 0$ are the nearest and next-to-nearest neighboring couplings, respectively. We train the CNN using the configurations of $g \stackrel{\text{def}}{=} J_2/|J_1| = 0.7$ and employ the resulting CNN to study the phase transition of $g = 0.8$. We find that this transfer learning is successful. In particular, only configurations of two temperatures, one is below and one is above the critical temperature T_c of $g = 0.7$, are needed to reach accurately determination of the T_c of $g = 0.8$. However, it may be subtle to use this strategy for the training. Specifically, for the considered model, due to the inefficiency of the single spin flip algorithm used in sampling the configurations at the low-temperature region, the two temperatures associated with the training set should not be too far away from the T_c of $g = 0.7$, otherwise, the performance of the obtained CNN is not of high quality, hence cannot determine the T_c of $g = 0.8$ accurately. For the considered model, we also uncover the condition for training a successful CNN when only configurations of two temperatures are considered as the training set.

I. INTRODUCTION

Recently, both the supervised and unsupervised neural networks (NN) have emerged as powerful methods of achieving understanding the critical phenomena of physical systems [1–6]. In particular, similar to the traditional ideas, these techniques can calculate with fair precision of both the critical points as well as the associated exponents. Despite the fact that the broad adoption of NN in exploring transitions between different phases took place only less than a decade ago, this modern approach paves a new route that may lead to understanding the critical phenomena from a different perspective.

Conventionally, when supervised NN is used to study a phase transition, both the configurations from below and above the critical points are employed to train the supervised NN. To achieve a valid NN that can determine the critical point with high accuracy, one may need certain amount of data and certain number of epochs to train the supervised NN. This training procedure typically consumes a lot of computing resources and time.

As a result, to advance the application of NN in investigating the critical phenomena, it is crucial and desirable to shorten the time for the training and to limit the use of computing resources. A highly efficient NN should be obtained at the same time as well.

There are some development in this regard. For instance, the transfer learning [7, 8], the use of theoretical ground states or artificially made configurations instead of real configurations for the training [9–11], the consideration of fewer neurons and layers [12], and so on.

Recently, the preprint of Ref. [13] argues that only the configurations of $T = 0$ and $T = \infty$ are required to train a successful supervised convolutional NN (CNN) to uncover the critical theory of the Ising model on the square lattice. Here T refers to the temperature. In Ref. [13], the configurations used for the training in principle are the theoretical ground state configurations. For example, all the Ising spins of the configurations of $T = 0$ used in the training stage take the same value of either 1 or -1. In addition, the configurations of $T = \infty$ are made random (in 1 and -1) manually. This approach is not different from the strategy of using ground state configurations as the training set which is firstly introduced in Ref. [9]. Finally, in Ref. [9], only the configurations of $T = 0$ are required and the data of $T = \infty$ are not needed for the training.

In studying the phase transition associated with the temperature of a real system, the data are determined experimentally within a temperature region. Therefore, if a phase transition is indeed observed in the considered temperature region of that experiment, then it will indeed be important and crucial to examine what is the minimal training set to obtain a supervised NN that is valid for investigating the targeted critical phenomenon.

We would like to emphasize the fact again that for experiments of a system that no any information of that system is known, it is impossible to employ the related theoretical ground states as the training set to train any NN. Therefore,

*fjjiang@ntnu.edu.tw

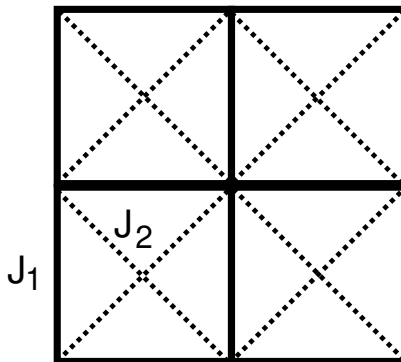


FIG. 1: The frustrated J_1 - J_2 Ising model on the square lattice studied here. The figure is taken from Ref. [29].

one can only rely on the real data to train a NN. Under such a circumstance, it is indeed necessary to examine what is the minimal training set (based on the experimental data) so that a resulting NN can successfully explore the desired phase transition.

One drawback of applying supervised NNs to study phase transitions is that the coarse location of the critical points should be available in advance before one can perform the NN calculations. If it is generally true that only the configurations (experimental data) at the two ends of the considered parameter are required to train a NN that works, then the rough position of the critical points is not necessary to conduct the supervised NN investigations. This will then put the supervised NNs at the same position of usefulness as their unsupervised counterparts.

To further examine the validity of the training strategy of using only the configurations at the two ends of the considered parameter, here we investigate the phase transitions of the frustrated J_1 - J_2 Ising model on the square lattice using three CNNs. Here $J_1 < 0$ and $J_2 > 0$ are the nearest and next-to-nearest neighboring couplings, respectively. This model has attracted a lot of theoretical and numerical interests during the last several decades due to its potential applications in frustrated magnets [14–29].

We train these CNNs using the configurations of $g \stackrel{\text{def}}{=} J_2/|J_1| = 0.7$, and then employ the obtained CNNs to calculate the critical temperature of $g = 0.8$.

Unexpectedly, although we do find only configurations of two temperatures, one is below and one is above the T_c of $g = 0.7$, are required to train a successful CNN that can calculate the T_c of $g = 0.8$ precisely, these two chosen temperatures cannot be too far away from the critical temperature of $g = 0.7$, otherwise, the T_c of $g = 0.8$ is either not accurately determined or receives fairly large finite-size effect(s).

By carefully examining the spin configurations in the training set(s), we also uncover the condition for training a successful CNN when only configurations of two temperatures are considered as the training set.

The rest of the paper is organized as follows. After the introduction which includes the motivation of current study, we detail the model and give a brief description of the used CNNs in Sect. II and Sect. III, respectively. Then the numerical outcomes are demonstrated thoroughly in Sect. IV. Finally, Sect. V contains our discussions and summaries of present investigation.

II. THE CONSIDERED MODEL

The Hamiltonian H of the frustrated J_1 - J_2 Ising model on the square lattice studied here has the following form

$$H = J_1 \sum_{\langle ij \rangle} \sigma_i \sigma_j + J_2 \sum_{\langle\langle lm \rangle\rangle} \sigma_l \sigma_m, \quad (1)$$

where $\sigma_i = \pm 1$ is the Ising spin at site i . The first and the second terms appearing in Eq. (1) are summed over nearest neighboring sites i and j and summed over next-to-nearest neighboring sites l and m , respectively. Fig. 1 is the graphical representation of the model studied here. In our calculations, $J_1 = -1$ and $g \stackrel{\text{def}}{=} J_2/|J_1|$. The phase transitions of $g = 0.7$ and $g = 0.8$ are investigated in this study.

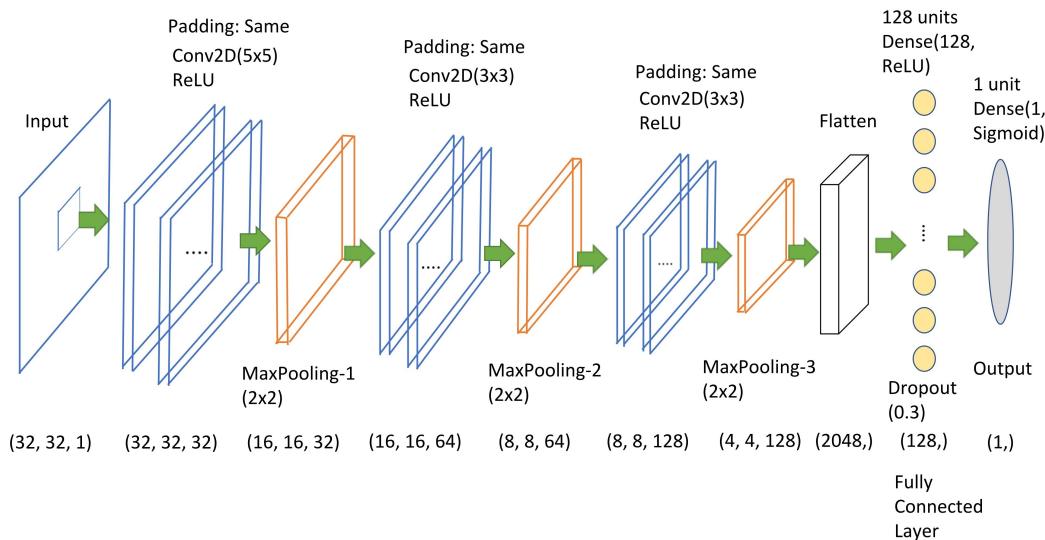


FIG. 2: The first CNN used here. The numbers at the bottom of the figure are for $L = 32$. The figure is created based on a figure of the submitted version of Ref. [30].

III. THE EMPLOYED CNNs

To ensure the claims found from the NN calculations do not depend on a specific architecture of the used CNN, in this study, we employ 3 different CNNs to investigate the proposed phase transitions. These CNNs are implemented using tensorflow and keras [31], and their architectures are introduced briefly in the following.

A. The first CNN

The architecture of the first CNN employed to study the targeted phase transition(s) is shown in fig. 2. The employed activation functions, the shape of kernels, the padding scheme, the pooling method, and other CNN-related parameters are explicitly shown in the figure. The epochs considered is 10. Moreover, the loss function used is the BinaryEntropy. Finally, the CNN outputs are real numbers from 0 to 1, and 0 and 1 stand for the likeness that the associated configurations are in the ordered and disordered phases, respectively. The training is conducted with configurations of $g = 0.7$ and the resulting CNN is considered to study the phase transition of $g = 0.8$. This first CNN is named CNN1 for convenience.

B. The second CNN

The second CNN used here is adopted from Ref. [30] and the associated pictorial representation of its architecture is depicted in fig. 3 (The architecture of the CNN of Ref. [30] is based on that of Ref. [32]). Moreover, the employed activation functions, the shape of kernels, the padding scheme, the pooling method, and other CNN-related parameters are explicitly shown in the figure. The CNN outputs are two-component vectors. The first and the second component of the CNN output stand for the likeness that the input configuration are in the ordered and disordered phases, respectively. This second CNN is named CNN2 for convenience.

Similar to CNN1, we use the configurations obtained with $g = 0.7$ to train CNN2. During the training, several sets of random seeds are used and 4 to 20 epochs are conducted. The typical values of loss function (we use CategoryEntropy as the loss function) during the training of performing 10 epochs are shown in fig. 4. The resulting CNN (CNN2) is then applied to study the phase transition of $g = 0.8$.

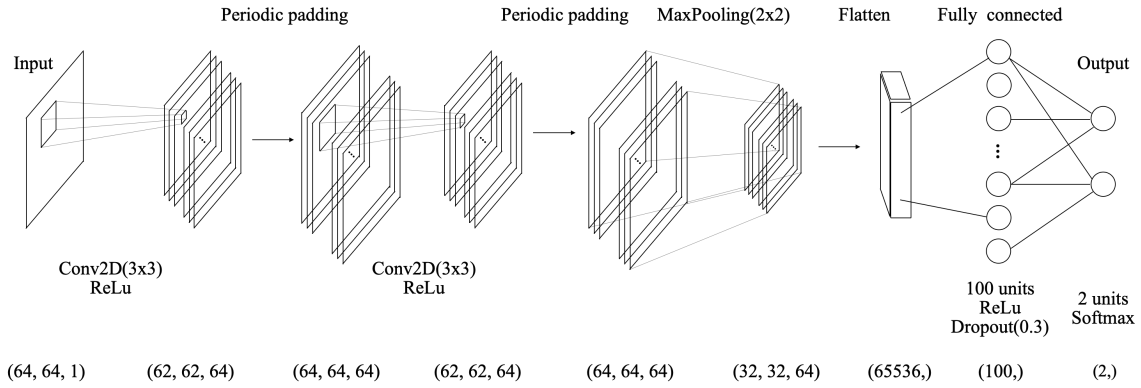


FIG. 3: The second CNN used here. The figure is taken from the submitted version of Ref. [30]. The numbers at the bottom of the figure are for $L = 64$.

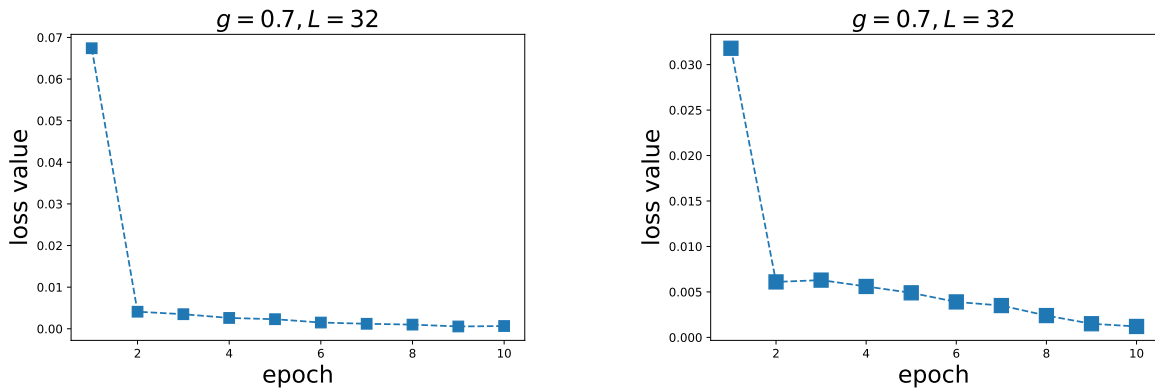


FIG. 4: The values of loss function during the training for conducting 10 epochs using CNN2.

C. The third CNN

The third CNN (which is denoted by CNN3 for convenience) considered here is two copies of CNN2. Specifically, the third CNN has two copies of the convolutional layers and the fully connected layer shown in fig. 3. In summary, CNN3 has four convolutional layers and two fully connected layers. The associated CNN3 outputs are two-component vectors like those of CNN2.

IV. NUMERICAL RESULTS

To study the proposed transfer learning and to investigate what is the minimal training set to train a CNN that works, for each of the chosen temperatures for both $g = 0.7$ and $g = 0.8$, we have generated few to several thousand configurations using single spin flip Metropolis algorithm [33]. It should be pointed out that for temperatures far below the critical temperature T_c , while one can reach one of the equilibrium steady ground states by the MC simulations, sampling among these states is difficult because the associated MC chain is generated by a local update algorithm. One notices this limitation is applied to both the cases of $g = 0.7$ and $g = 0.8$. Therefore, if the associated configurations obtained from the simulations at the low-temperature region of $g = 0.7$ are considered in the training set(s), then apparently the resulting CNN can identify the configurations of the low- T region of $g = 0.8$. Evidence supporting this fact will be demonstrated later when the CNN outcomes are presented. As a result, both the low- T configurations of $g = 0.7$ and $g = 0.8$ are included in our investigation.

We would like to emphasize the fact again that the training is performed using the configurations of $g = 0.7$ and the resulting trained CNN is used to study the phase transition associated with $g = 0.8$. Finally, it should be pointed out that the T_c of $g = 0.7$ and $g = 0.8$ are given by 1.2890 and 1.5678, respectively [25, 28, 29].

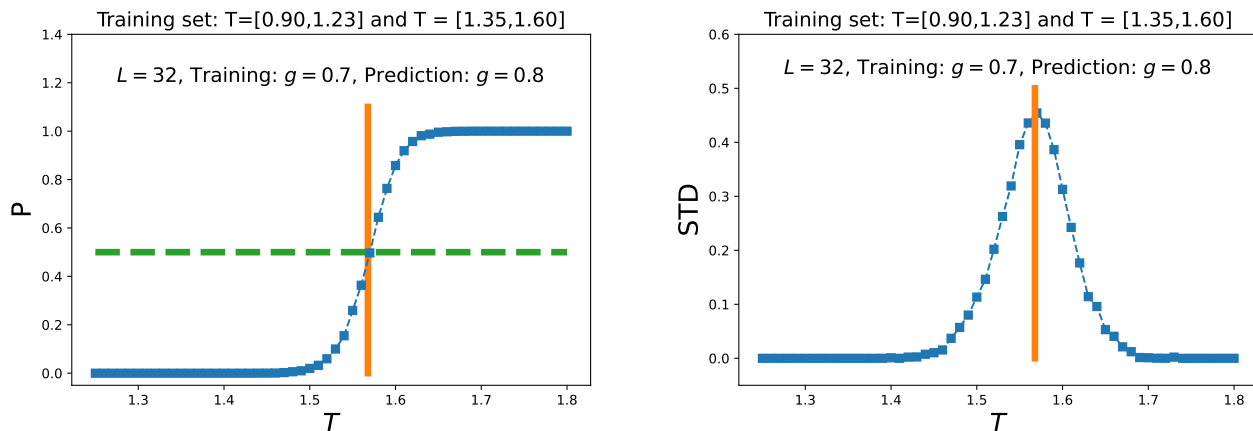


FIG. 5: The transfer learning results. (Left) The NN outputs as a function of T . The horizontal dashed line is 0.5. (Right) The associated standard deviations (STD) as a function of T . In both panels, the vertical solid lines are the theoretical T_c of $g = 0.8$. These outcomes are associated with CNN1.

A. The outcomes related to CNN1

The left panel of fig. 5 demonstrates the outputs of CNN1 as a function of T for $g = 0.8$ with $L = 32$. The title shows the temperatures considered for the training. In the training set, we excluded those configurations which the associated temperatures are near T_c . In the figure, the horizontal dashed and vertical solid lines represent 0.5 and the T_c of $g = 0.8$. The intersection of the outputs and 0.5 is the NN-determined critical temperature. As can be seen from the panel, the NN-determined critical temperature agrees very well with the theoretical T_c .

The STD of the NN outputs as a function of T is depicted in the right panel of fig. 5. The panel reveals the message that at T_c , the magnitude of the STD of NN output is the largest.

To summarize, both the NN outputs and the associated STD can be employed to calculate the NN-related T_c with fairly high accuracy.

Despite the fact that the configurations obtained at low- T region may not have all the degenerated stripe states (due to the inefficiency of the single spin flip algorithm used here), the outcomes demonstrated in fig. 5 provide evidence supporting the effectiveness of including these low- T configurations in the CNN calculations.

Fig. 6 shows the CNN1 outputs as a function of T for $g = 0.8$ when the configurations of $T = 1.25$ and $T = 1.33$ of $g = 0.7$ are used as the training set. Moreover, the diamond symbols in the figure represent these two temperatures and the vertical dashed line is the T_c of $g = 0.7$. The vertical solid line is the expected T_c of $g = 0.8$. The results of the figure demonstrate that when the training set consists of merely configurations from two temperatures, the obtained CNN1 can successfully determine the T_c of $g = 0.8$ precisely.

Fig. 7 shows the CNN1 outputs as functions of T for $g = 0.8$ when the configurations of two temperatures of $g = 0.7$ are used as the training sets (The used temperatures are listed as the titles of the panels and are presented as the diamond symbols in the figure). The horizontal dashed, the vertical dashed, and the vertical solid lines are 0.5, T_c of $g = 0.7$, and T_c of $g = 0.8$, respectively. As can be seen from all the panels of the figure, when one of (both) the temperatures is (are) far away from the T_c of $g = 0.7$, then one reaches poor determination of the T_c of $g = 0.8$ using the resulting CNN1.

Similarly, when both the chosen temperatures are below or are above the T_c of $g = 0.7$, the obtained CNN1 cannot calculate the T_c of $g = 0.8$ with high accuracy or the estimated T_c receives a very large finite-size effect, see both panels of fig. 8

Fig. 9 shows the CNN1 outputs as a function of T when the training set only contains the configurations of $T = 0.1$ and $T = 10.0$ of $g = 0.7$. The outcomes of the figure indicate the outputs jump between 1 and 0 at the low- T region. This phenomenon is also found in figs. 7 and 8.

The typical snapshots of spin configurations for $T = 0.1$ of $g = 0.7$, $T = 1.25$ of $g = 0.8$, and $T = 1.26$ of $g = 0.8$ are depicted as the left, the middle and the right panels of Fig. 10. Clearly, one observes high similarity between the left and the middle panels, hence leads to a CNN1 output around 0. On the other hand, the left and the right panels are in strong contrast to each other, and one expects the CNN1 output to be around 1. In other words, the results at the low- T region shown in fig. 9 (see the right panel of this figure) agree well with the expectations from the snapshots of fig. 10. In particular, the phenomenon of CNN1 outputs jumping between 1 and 0 can be understood well from the

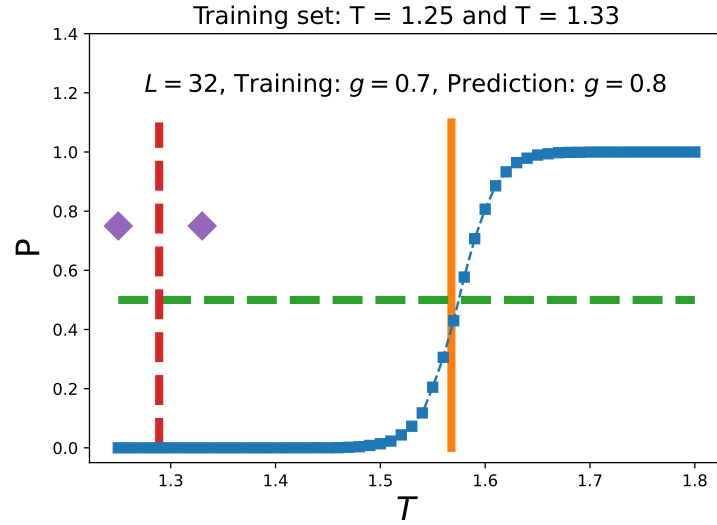


FIG. 6: The transfer learning results. The CNN1 outputs as a function of T . The horizontal dashed line is 0.5. The training set consists of configurations of $T = 1.25$ and $T = 1.33$ (The diamond symbols). The vertical dashed and solid lines are the theoretical T_c of $g = 0.7$ and $g = 0.8$, respectively. These outcomes are associated with CNN1

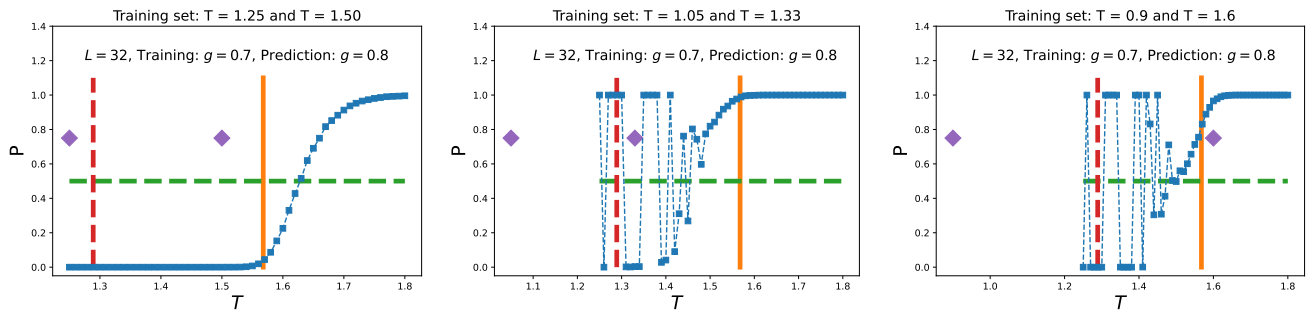


FIG. 7: The transfer learning results. The CNN1 outputs as functions of T . The horizontal dashed lines are 0.5. Diamond symbols represent the temperatures for which the associated configurations are considered in the training sets. The vertical dashed and solid lines are the theoretical T_c of $g = 0.7$ and $g = 0.8$, respectively. These outcomes are associated with CNN1.

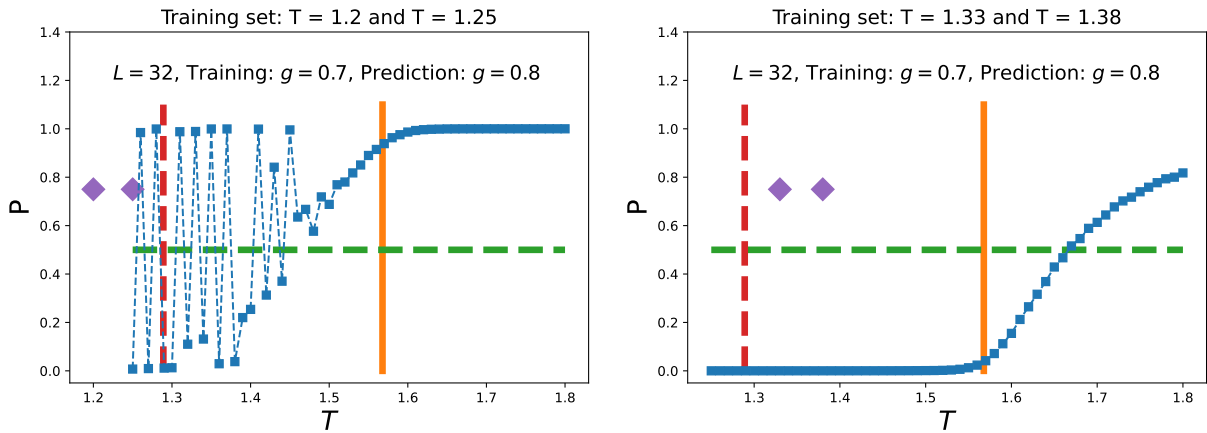


FIG. 8: The transfer learning results. The CNN1 outputs as functions of T . The horizontal dashed lines are 0.5. Diamond symbols represent the temperatures for which the associated configurations are considered in the training sets. The vertical dashed and solid lines are the theoretical T_c of $g = 0.7$ and $g = 0.8$, respectively. These outcomes are associated with CNN1.

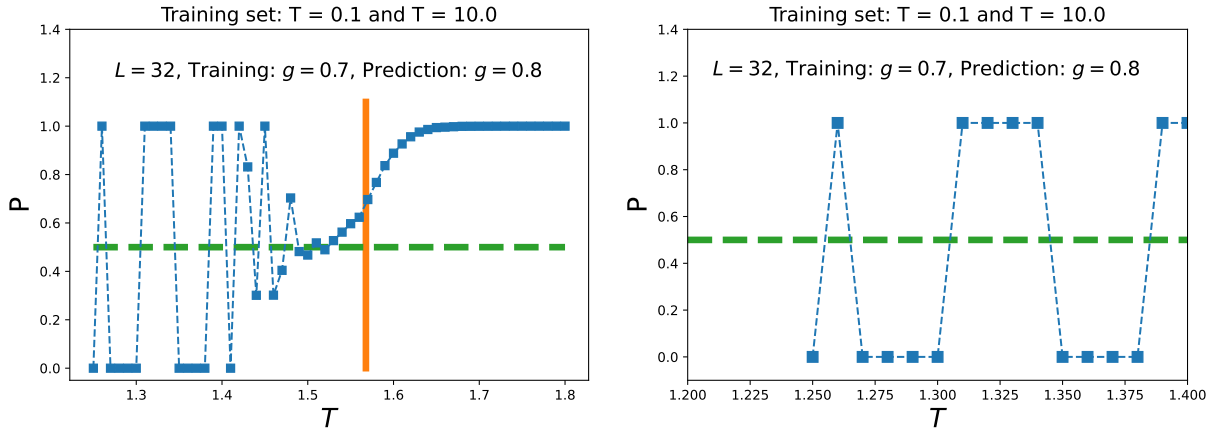


FIG. 9: The transfer learning results. (Left) The CNN1 outputs as a function of T . The horizontal line is 0.5. The training set consists of configurations of $T = 0.1$ and $T = 10.0$. The vertical solid line is the theoretical T_c of $g = 0.8$. (Right) The zoom in results of the left panel.

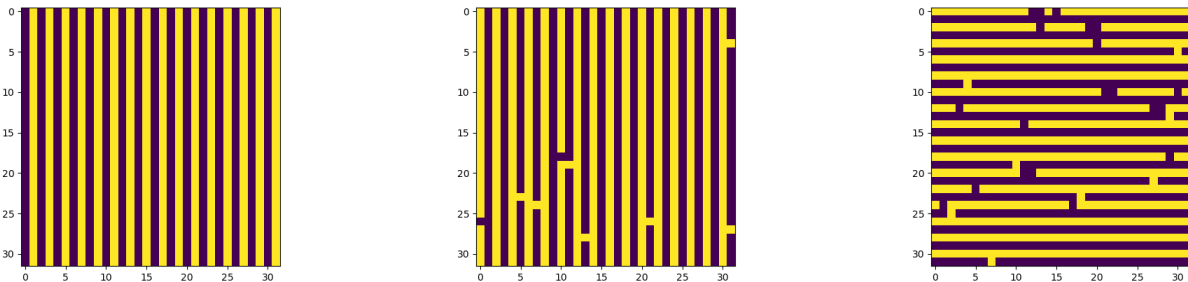


FIG. 10: Typical snapshots of spin configurations for $T = 0.1$ of $g = 0.7$ (left), $T = 1.25$ of $g = 0.8$ (middle), and $T = 1.26$ of $g = 0.8$ (right). These outcomes are associated with CNN1.

snapshots of the spin configurations. Hence, the inclusion of the configurations at low- T region in the training set is thus legitimate, and the outputs from the resulting CNN1 are fully consistent with the associated snapshots of the underlying spin configurations.

Since in this situation the P curve jumps between 0 and 1 in the low-temperature region and becomes stable for those T that are larger than a particular value of temperature T_p , one may take the T_p as the pseudo-critical temperature.

One notices that the determined values of T_p in the two most right panels of figs. 7, the left panel of fig. 8, and fig. 9 are far away from the expected T_c , implying less accurate determination of T_c compared to that of fig. 5.

B. The outcomes related to CNN2

The left panel of fig. 11 shows the two components of the CNN2 outputs as functions of T . At what temperatures is the training carried out is shown as the title of the panel. The title of the panel shows that the temperatures near the T_c of $g = 0.7$ are excluded from being considered in the training set. Finally, the vertical line is the expected T_c of $g = 0.8$. As can be seen from the panel, the temperature where the two components intersect agrees very well with the expected T_c of $g = 0.8$. This provides evidence to support the success of the proposed transfer learning using CNN2.

The right panel of fig. 11 demonstrates the standard deviations (STD) of the first component of the CNN outputs as a function of T . The results of the panel indicate that the temperature having the largest STD matches excellently with the T_c of $g = 0.8$. Hence, similar to the results related to CNN1, both the intersection and STD associated with CNN2 can be considered as indicators to determine the critical temperature.

Finally, based on the CNN2 outcomes, shown in fig. 11, it is evident that the inclusion of the configurations of

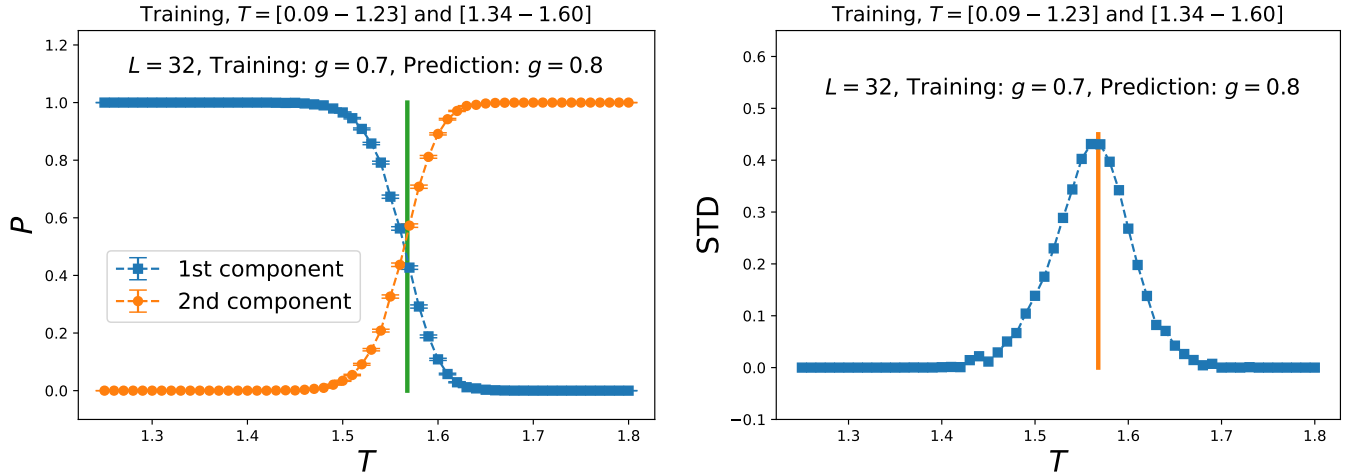


FIG. 11: The transfer learning results. (Left) The first and the second components of the CNN2 outputs as functions of T . (Right) The associated standard deviations (STD) of the first component (of the CNN2 outputs) as a function of T . The vertical solid lines in both panels are the theoretical T_c of $g = 0.8$.

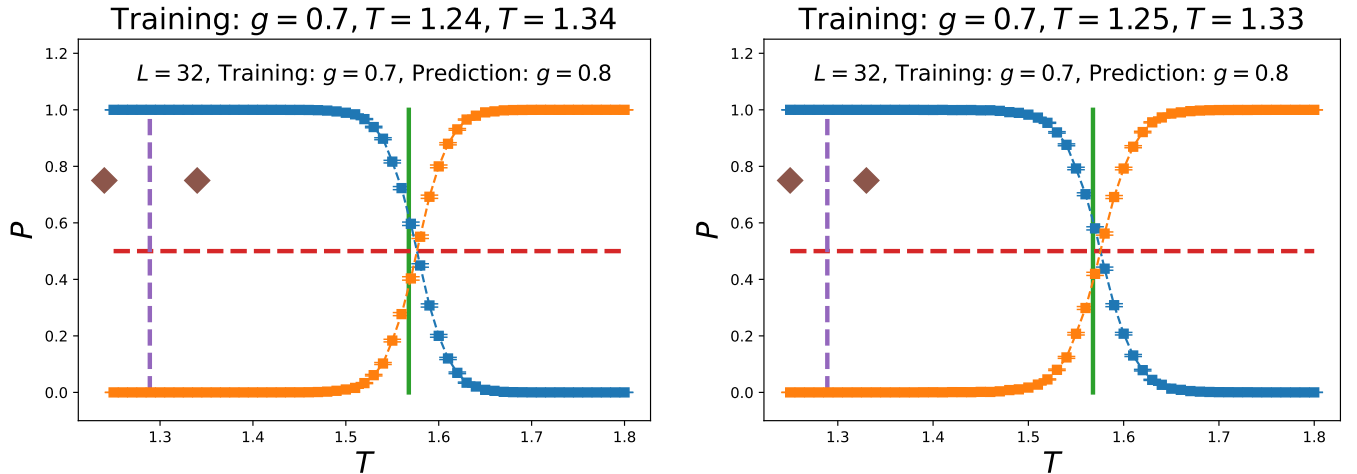


FIG. 12: The transfer learning results of using configurations at two temperatures as the training set. The diamond symbols, the dashed vertical lines, and the solid vertical lines represent the temperatures associated with training, T_c of $g = 0.7$, and T_c of $g = 0.8$, respectively. These outcomes are associate with CNN2.

low- T region of $g = 0.7$ in the training set(s) indeed can lead to a accurate determination of the T_c of $g = 0.8$.

Interestingly, we do find that only configurations at two temperatures are required to train a successful CNN2. Both panels in fig. 12 and the left panel of fig. 13 show the CNN2 outputs as functions of T for $L = 32$ and $g = 0.8$. The diamond symbols in these panels represent the temperatures for which the associated configurations are used as the training set. The vertical bold dashed and bold solid lines stand for the values of T_c for $g = 0.7$ and $g = 0.8$, respectively, and the bold horizontal dashed line is 0.5. It is clear that when the CNN2 is trained with configurations of merely two temperatures, one is above and one is below the T_c of $g = 0.7$ and those temperatures are not too far away from the T_c of $g = 0.7$, the intersection of the two components of the CNN2 output vectors for $g = 0.8$ obtained from the trained CNN2 matches well with the T_c of $g = 0.8$.

With the same notations and conventions introduced in the previous paragraph, the right panel of fig. 13, both panels of figs. 14 suggest that if any of the chosen two temperatures, for which the associated configurations are used as the training set, is too far away from the T_c of $g = 0.7$, then the trained CNN2 either fails to determine the T_c of $g = 0.8$ accurately (the left panel of fig. 14) or the NN-calculated value of T_c is far away from the theoretical one (the right panel of fig. 14). If in the right panel of fig. 13 and in the right panel of fig. 14, one takes the most right

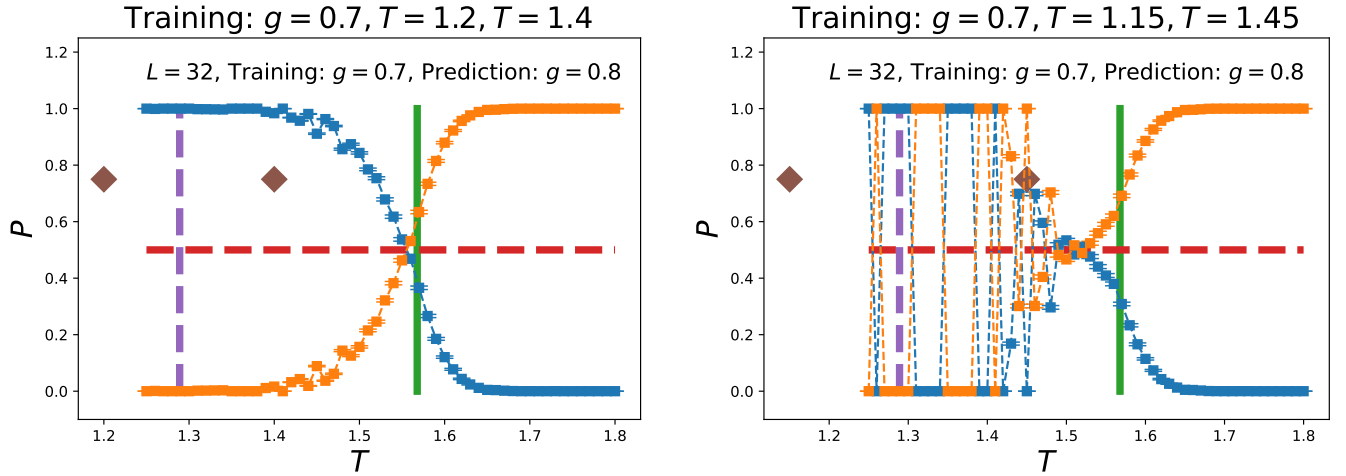


FIG. 13: The transfer learning results of using configurations at two temperatures as the training set. The diamond symbols, the bold dashed vertical lines, and the bold solid vertical lines represent the temperatures associated with training, T_c of $g = 0.7$, and T_c of $g = 0.8$, respectively. The bold horizontal dashed line is 0.5. These outcomes are associated with CNN2.

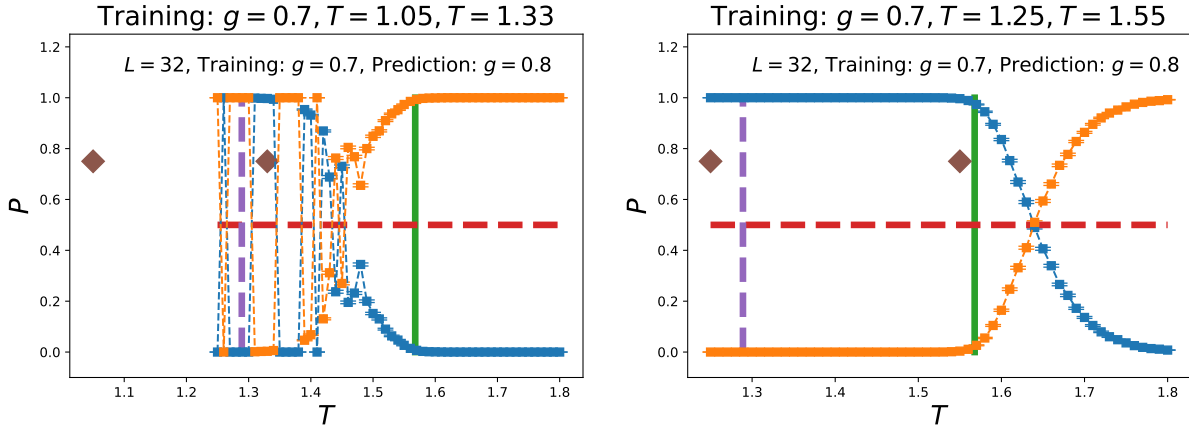


FIG. 14: The transfer learning results of using configurations at two temperatures as the training set. The diamond symbols, the bold dashed vertical lines, and the bold solid vertical lines represent the temperatures associated with training, T_c of $g = 0.7$, and T_c of $g = 0.8$, respectively. The bold horizontal dashed line is 0.5. These outcomes are associated with CNN2.

intersecting point associated with the two components of the CNN2 outputs as the NN-determined T_c , then clearly the NN-determined values of T_c are away from the theoretical T_c and are less accurate than those estimated in figs. 11 and 12.

Similarly, if the chosen two temperatures are both below or are both above the T_c of $g = 0.7$, then the resulting CNN2 either fails to determine the T_c of $g = 0.8$ accurately or the NN-calculated T_c is far away from the theoretical T_c , see fig. 15

Finally, the CNN2 outputs as functions of T obtained by conducting 100 epochs for the training and using 3 different sets of random seeds are depicted in fig. 16. The training set consists of the configurations of $T = 0.1$ and $T = 10.0$ of $g = 0.7$. The outcomes of fig. 16 reveal the same message as those show previously. In particular, if the temperature where both the P curves become stable is treated as the NN-determined pseudo-critical temperature, then one finds that while the NN-calculated values of T_c for $g = 0.8$ are close to the theoretical one, they are less accurate than those shown in figs. 11, 12 and 13.

It is also important to point out that the fluctuations appeared in the low- T region in some of the figures can be explained well by the snapshots of fig. 10. In other words, the inclusion of the low- T configurations in the training set is legitimate and can indeed capture the characteristics of states in the testing set(s).

Previously, the outcomes from CNN2 are for $L = 32$. In the following, certain results associated with $L = 128$ will

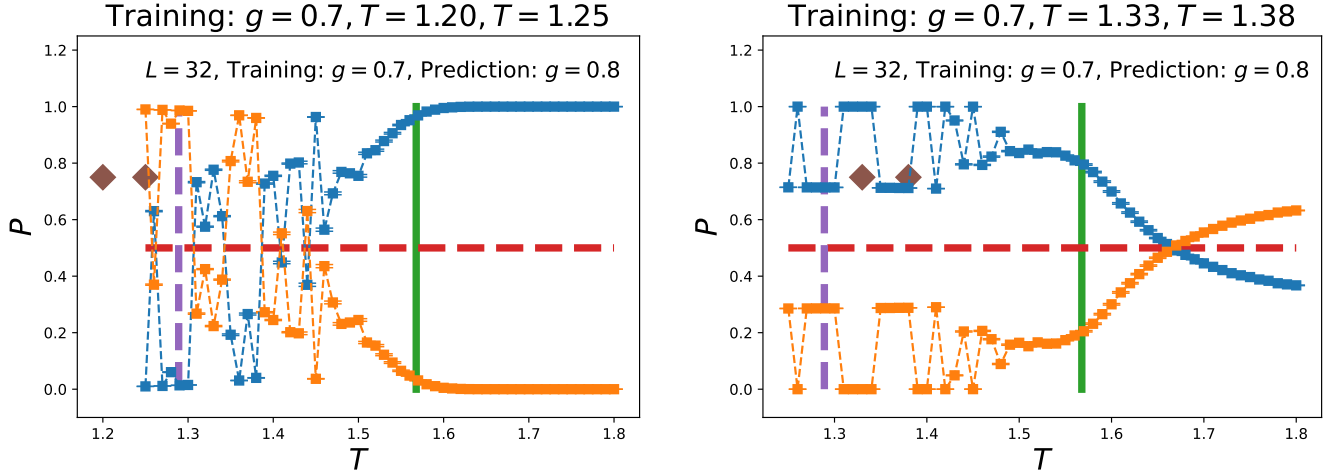


FIG. 15: The transfer learning results of using configurations at two temperatures as the training set. The diamond symbols, the bold dashed vertical lines, and the bold solid vertical lines represent the temperatures associated with training, T_c of $g = 0.7$, and T_c of $g = 0.8$, respectively. The bold horizontal dashed line is 0.5. These outcomes are associated with CNN2.

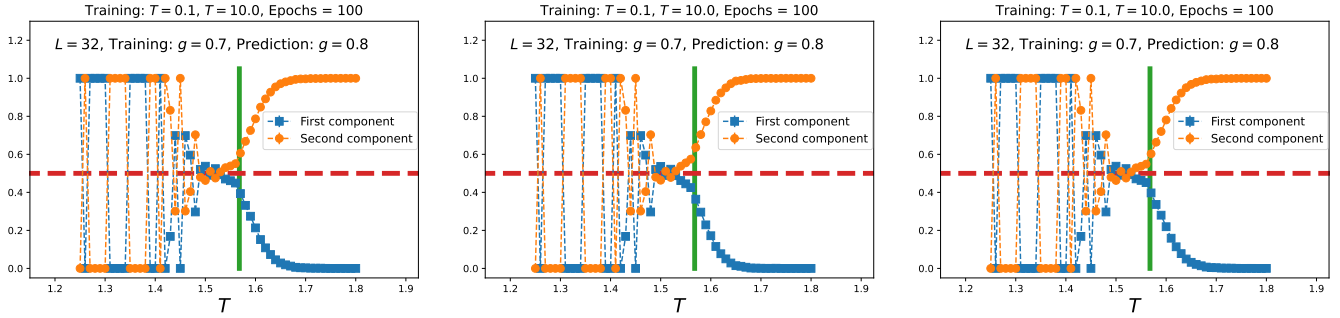


FIG. 16: The transfer learning results of using configurations at two temperatures, namely $T = 0.1$ and $T = 10.0$, as the training set. The bold solid vertical line and the bold horizontal lines represent T_c of $g = 0.8$ and 0.5, respectively. The number of epochs considered for obtaining these results is 100 and each panel is determined with the CNN2 trained by using different sets of random seeds.

be demonstrated.

The left and the right panels of fig. 17 are the NN results for $g = 0.8$ with $L = 128$ and are obtained using CNN2. Both the training processes consider configurations of two temperatures (of $g = 0.7$) and the used temperatures are listed as the titles of the panels. If the most right intersecting points are treated as the CNN-determined pseudo-critical temperatures, then beyond doubt the training with $T = 1.24$ and $T = 1.34$ receives (much) less finite-size effect than that of the training with $T = 0.1$ and $T = 10.0$. Here again, the fluctuations between 0 and 1 for the two components of the NN outputs below T_c are due to the same reason as that explaining the fluctuations shown up in figs. 7, 8, and 9, see fig. 18 and the associated caption.

Indeed, the similarity between the left ($T = 1.24, g = 0.7$) and the right ($T = 1.49, g = 0.8$) panels of fig. 18 definitely will lead to a CNN2 output vector with the first component being around 1. In addition, based on the strong contrast between the left ($T = 1.24, g = 0.7$) and the middle ($T = 1.52, g = 0.8$) panels, one would arrive at a CNN2 output vector with the first component being around 0. These arguments agrees well with the results presented in the left panel of fig. 17.

The separation between two consecutive temperatures in the testing set resulting in fig. 17 is $\Delta T = 0.01$. If one considers smaller ΔT , namely $\Delta T = 0.002$, then the results from CNN2 are depicted in fig. 19. Similarly, if the most right intersecting points are treated as the CNN-determined pseudo-critical temperatures, then beyond doubt the training with $T = 1.24$ and $T = 1.34$ receives less finite-size effect than that of the training with $T = 0.1$ and $T = 10.0$.

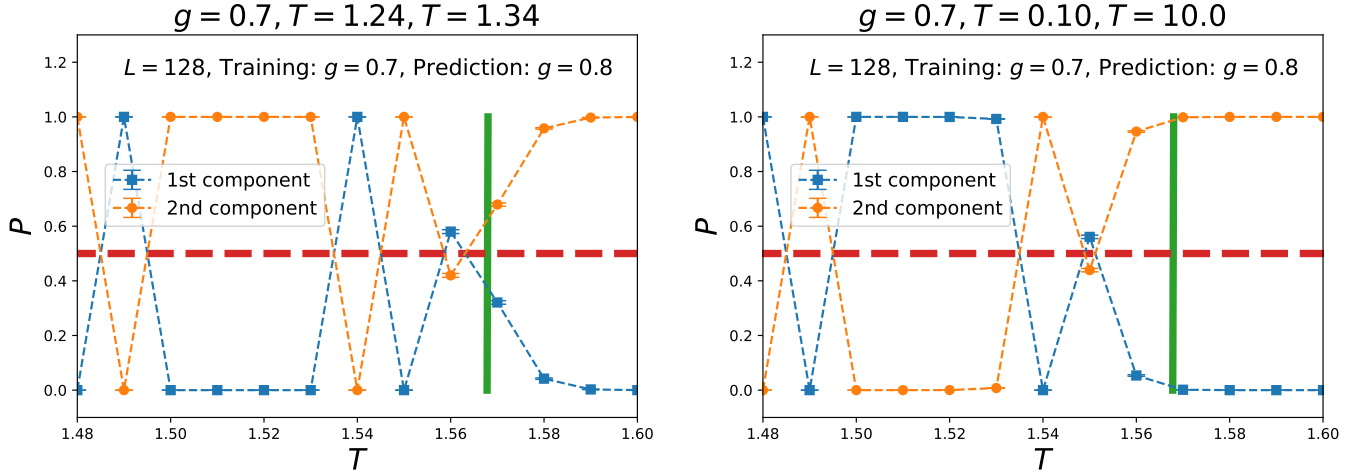


FIG. 17: The transfer learning results of using configurations at two temperatures, namely $T = 1.24$ and $T = 1.34$ (left panel), as the training set. The separation between two consecutive temperatures in the testing set (denoted by ΔT) is 0.01. The bold solid vertical line and the bold horizontal dashed lines represent T_c of $g = 0.8$ and 0.5, respectively. The number of epochs considered for obtaining these results is 100. The outcomes are obtained using CNN2. The NN-related parameters for outcomes of the right panel are the same as those of the left panel, except that the two temperatures related to the training are 0.1 and 10.0.

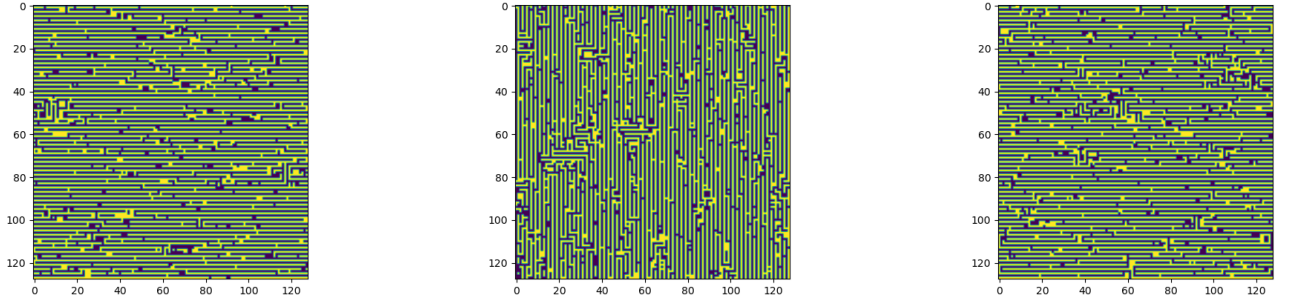


FIG. 18: Typical snapshots of spin configurations for $T = 1.24$ of $g = 0.7$ (left), $T = 1.52$ of $g = 0.8$ (middle), and $T = 1.49$ of $g = 0.8$ (right).

C. The outcomes related to CNN3

For the last CNN3 considered here, we have focused on the linear system size $L = 128$.

For the separation between two consecutive temperatures in the testing set being $\Delta T = 0.01$, the outcomes associated with CNN3 are demonstrated in fig. 20.

The left and the right panels are the NN results for $g = 0.8$ with $L = 128$. Both the training processes consider configurations of two temperatures (of $g = 0.7$) and the used temperatures are listed as the titles of the panels. If the most right intersecting points are treated as the CNN-determined pseudo-critical temperatures, then beyond doubt that the training with $T = 1.24$ and $T = 1.34$ receives less severe finite-size effect than that of the training with $T = 0.1$ and $T = 10.0$.

If one considers the case of $\Delta T = 0.002$, then the results from CNN3 are depicted in fig. 21. Similarly, if the most right intersecting points are treated as the CNN-determined pseudo-critical temperatures, then beyond doubt the training with $T = 1.24$ and $T = 1.34$ receives less severe finite-size effect than that of the training with $T = 0.1$ and $T = 10.0$.

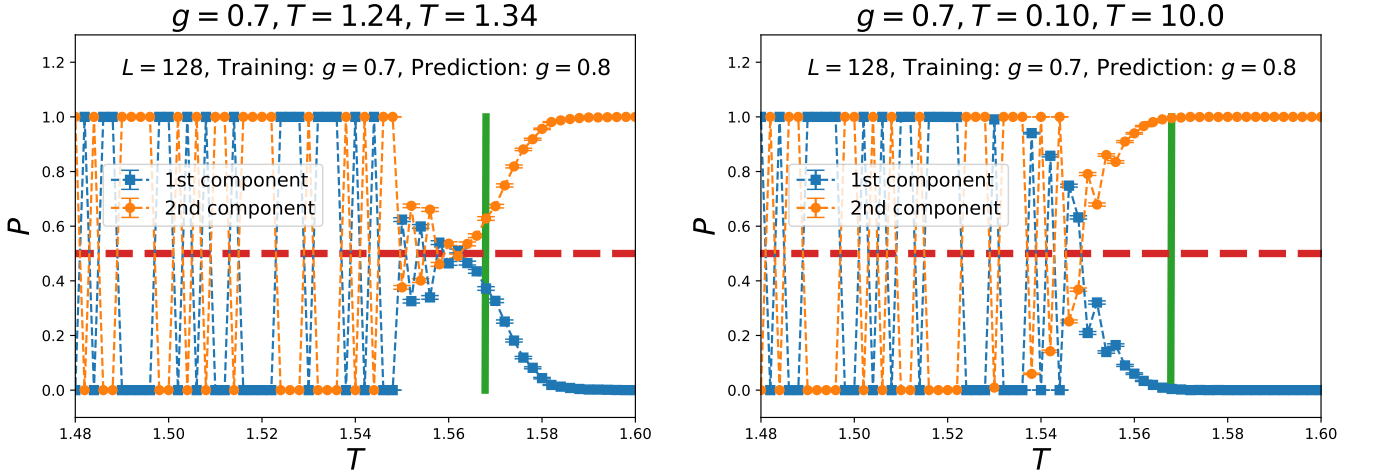


FIG. 19: The transfer learning results of using configurations at two temperatures, namely $T = 1.24$ and $T = 1.34$ (left panel), as the training set. $\Delta T = 0.002$. The bold solid vertical line and the bold horizontal dashed lines represent T_c of $g = 0.8$ and 0.5 , respectively. The number of epochs considered for obtaining these results is 100. The outcomes are obtained using CNN2. The NN-related parameters for outcomes of the right panel are the same as those of the left panel, except that the two temperatures related to the training are 0.1 and 10.0 . The outcomes of both panels are obtained using CNN2.

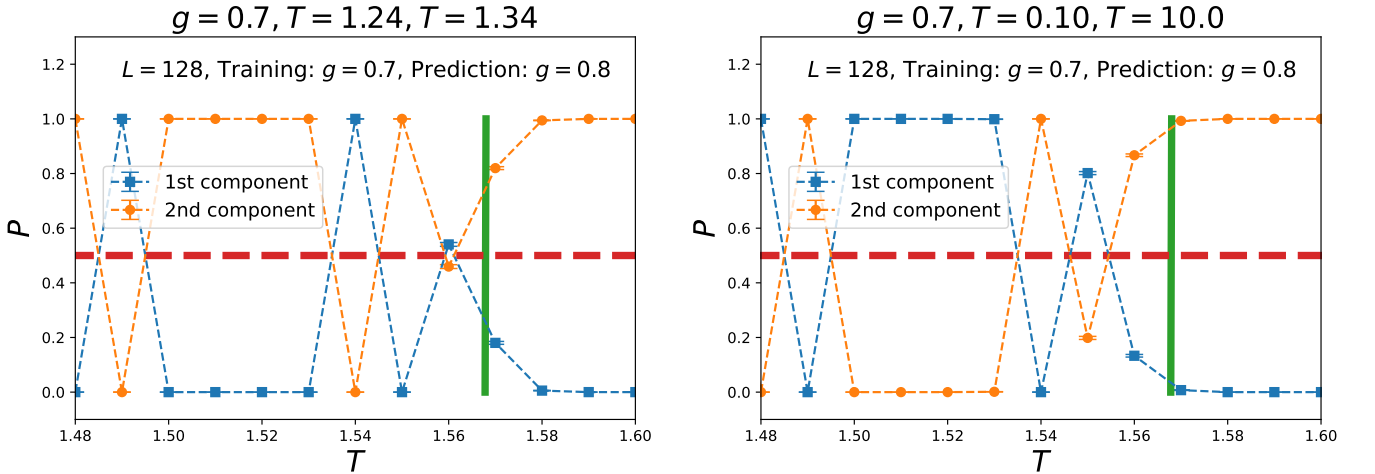


FIG. 20: The transfer learning results of using configurations at two temperatures, namely $T = 1.24$ and $T = 1.34$ (left panel), as the training set. $\Delta T = 0.01$. The bold solid vertical line and the bold horizontal lines represent T_c of $g = 0.8$ and 0.5 , respectively. The number of epochs considered for obtaining these results is 100. The NN-related parameters for the outcomes of the right panel are the same as those of the left panel, except that the two temperatures related to the training are 0.1 and 10.0 . The outcomes of both panels are obtained using CNN3.

V. DISCUSSIONS AND CONCLUSIONS

In this study, we examine the transfer learning for the frustrated J_1 - J_2 Ising model on the square lattice. Specifically, we train three CNNs using the spin configurations of $g = 0.7$ as the training set. Then the obtained CNNs are employed to study the phase transition of $g = 0.8$.

We find that this transfer learning is successful. In particular, only configurations of two temperatures, one is below and one is above the T_c of $g = 0.7$, are needed to train a working CNN that can determine the critical temperature T_c of $g = 0.8$ precisely.

We also find that the chosen two temperatures mentioned in the previous paragraph, which are used for the training, cannot be too far away from the T_c of $g = 0.7$, otherwise, the obtain CNN cannot calculate the wanted T_c of $g = 0.8$

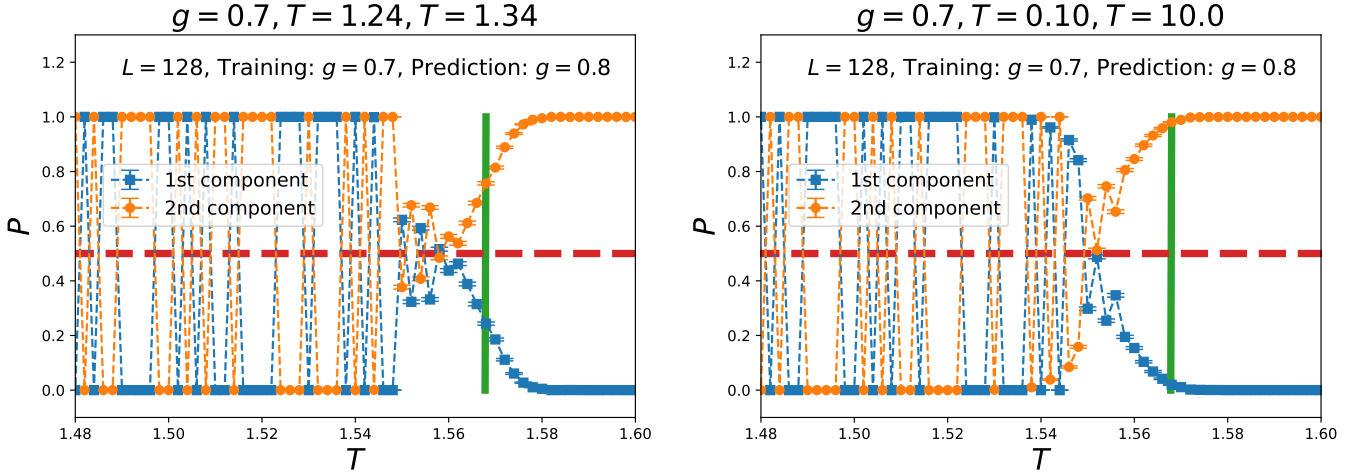


FIG. 21: The transfer learning results of using configurations at two temperatures, namely $T = 1.24$ and $T = 1.34$ (left panel), as the training set. $\Delta T = 0.002$. The bold solid vertical line and the bold horizontal lines represent T_c of $g = 0.8$ and 0.5 , respectively. The number of epochs considered for obtaining these results is 100. The outcomes are obtained using CNN3. The NN-related parameters for outcomes of the right panel are the same as those of the left panel, except that the two temperatures related to the training are 0.1 and 10.0 . The outcomes are obtained using CNN3.

with reasonably high precision. Specially, a large finite-size effect is observed.

In addition, despite the fact that the configurations at low- T region do not contain all the possible ground state configurations, we find they can still be considered in the training and prediction stages, with the price of the appearance of large finite-size effects.

The model considered here have been studied in Refs. [7, 34] using a supervised CNN (with transfer learning) and an unsupervised variational auto-encoder. Configurations at multiple temperatures, both (far) below and above the T_c , are considered as the training set(s) in these two studies. As a result, it is likely that the training sets of [7, 34] contain biased states like ours since local spin flip algorithms are used in Refs. [7, 34]. However, similar to our outcomes shown in figs. 5 and 11, satisfactory results are obtained in these two references since the role of biased configurations at low- T region in the training stage are tamed by the configurations below but near T_c .

Because the training process is the most time-consuming procedure in a NN study of critical phenomena, it is indeed desirable to obtain a strategy of shortening the time and reducing the computing resources required to train a NN. The idea of employing as few spin configurations as possible in the training set is one route to reach this goal. In addition, using configurations from temperatures far away from the critical points makes the supervised training procedure be similar to the unsupervised ones. Our investigation presented here demonstrates that the use of real configurations (not the theoretical ones) from $T = 0$ and $T = \infty$ as the training set may seriously sacrifice the accuracy of the determined critical points (hence the critical exponents). As a result, in a NN calculation, the method of using only the real configurations at the two ends of the considered parameter as the training set may not be an ideal approach since one may not reach very high precision for the critical points and exponents with such a training strategy.

Of course, our conclusions are based on the fact that the MC algorithm used here is not able to sample the configurations at low- T region efficiently. Hence, the observed large finite-size effect(s) and the phenomenon of the CNN outputs jumping between 0 and 1 may attribute to this. For real experiments, it can be the case that the data at the two ends of the considered parameter may be sufficient to train a CNN successfully so that it can determine the critical points and the associated exponents with acceptable accuracy. This success crucially relies on the condition that the data at the two ends of the considered parameter contain (almost) all the information (all the possible states) of the studied system.

To understand the success of determining the T_c accurately as that shown in the right panel of fig. 12 (Which uses only configurations of $T = 1.25$ and $T = 1.33$ as the training set), we have investigated the spin configurations of $T = 1.25$. Interestingly, we do find that the training set contains configurations similar to the four expected ground state stripe configurations, see fig. 22. This outcome provides convincing evidence to support our claim made in the previous paragraph. Specifically, the training of a NN would be successful if the data at the two ends of the considered parameter contain (almost) all the information (all the possible states) of the studied system. Finally, the left panel of fig. 7 and the right panel of fig. 14 suggest that the separation between the high end parameter and the true T_c

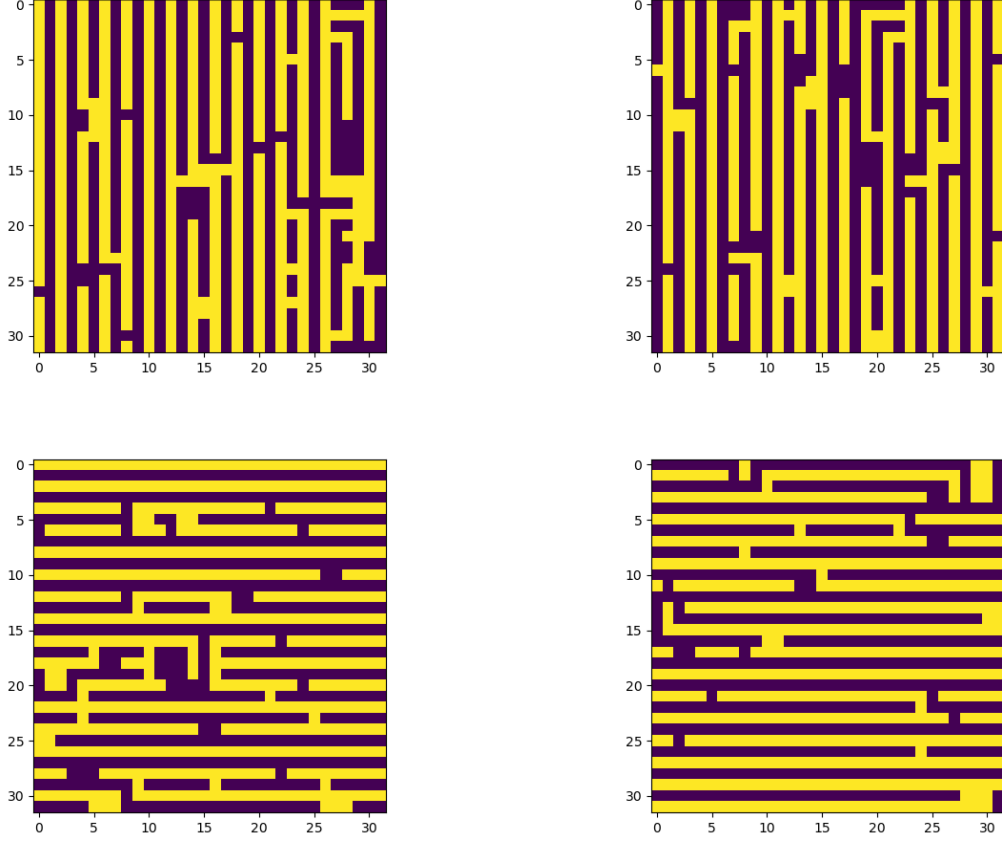


FIG. 22: The snapshots of $g = 0.7$ with $L = 32$ and $T = 1.25$.

cannot be too larger than that associated with the low end parameter as well.

In conclusion, conducting the required NN calculations is needed to determine whether the idea of using the data at the two ends of the considered parameter can lead to a NN that can be used to explore the wanted critical phenomenon accurately. In particular, it is crucial that the data at the low end of the considered parameter should contain all the possible ground-state like configurations, and the separation between one end of the studied parameter and the true T_c cannot differ too much from that related to the other end of parameter, to ensure a successful training.

Funding

Partial support from National Science and Technology Council (NSTC) of Taiwan is acknowledged (Grant numbers: NSTC 112-2112-M-003-016- and NSTC 113-2112-M-003-014-).

Conflict of Interest

The authors declare no conflict of interest.

Data Availability Statement

Data are available from the corresponding author on reasonable request.

-
- [1] Tomoki Ohtsuki and Tomi Ohtsuki, *Deep Learning the Quantum Phase Transitions in Random Two-Dimensional Electron Systems*, J. Phys. Soc. Jpn. **85**, 123706 (2016).
- [2] Akinori Tanaka, Akio Tomiya, *Detection of Phase Transition via Convolutional Neural Networks*, J. Phys. Soc. Jpn. **86**, 063001 (2017).
- [3] Juan Carrasquilla, Roger G. Melko, *Machine learning phases of matter*, Nature Physics **13**, 431–434 (2017). (2017). <https://doi.org/10.1038/nphys4035>.
- [4] Evert P.L. van Nieuwenburg, Ye-Hua Liu, Sebastian D. Huber, *Learning phase transitions by confusion*, Nature Physics **13**, 435–439 (2017). <https://doi.org/10.1038/nphys4037>.
- [5] P. Mehta, M. Bukov, C.-H. Wang, A. G.R. Day, C. Richardson, C. K. Fisher and D. J. Schwab, *A high-bias, low-variance introduction to machine learning for physicists*, Phys. Rep. **810**, 1 (2019). <https://doi.org/10.1016/j.physrep.2019.03.001>.
- [6] G. Carleo, I. Cirac, K. Cranmer, L. Daudet, M. Schuld, N. Tishby, L. Vogt-Maranto and L. Zdeborová, *Machine learning and the physical sciences*, Rev. Mod. Phys. **91**, 045002 (2019). <https://doi.org/10.1103/RevModPhys.91.045002>.
- [7] I. Corte, S. Acevedo, M. Arlego, C.A. Lamas, *Exploring neural network training strategies to determine phase transitions in frustrated magnetic models*, Computational Materials Science **198** (2021) 110702. <https://doi.org/10.1016/j.commatsci.2021.110702>.
- [8] Kimihiko Fukushima and Kazumitsu Sakai, *Can a CNN trained on the Ising model detect the phase transition of the q-state Potts model?*, Prog. Theor. Exp. Phys. **2021**, 061A01. <https://doi.org/10.1093/ptep/ptab057>.
- [9] C.-D. Li, D.-R. Tan, and F.-J. Jiang, *Applications of neural networks to the studies of phase transitions of two-dimensional Potts models*, Annals of Physics, **391** (2018) 312-331. <https://doi.org/10.1016/j.aop.2018.02.018>.
- [10] D.-R. Tan *et al.* *A comprehensive neural networks study of the phase transitions of Potts model*, 2020 New J. Phys. **22** 063016, 1-17. <https://doi.org/10.1088/1367-2630/ab8ab4>.
- [11] D.-R. Tan and F.-J. Jiang, *Machine learning phases and criticalities without using real data for training*, Phys. Rev. B **102**, 224434 (2020). <https://doi.org/10.1103/PhysRevB.102.224434>.
- [12] Dong-kyu Kim and Dong-Hee Kim, *Smallest neural network to learn the Ising criticality*, Phys. Rev. E **98**, 022138 (2018). <https://doi.org/10.1103/PhysRevE.98.022138>.
- [13] Ahmed Abuali, David A. Clarke, Morten Hjorth-Jensen, Ioannis Konstantinidis, Claudia Ratti, Jianyi Yang, *Deep learning of phase transitions with minimal examples*, arXiv:2501.05547. <https://doi.org/10.48550/arXiv.2501.05547>.
- [14] K. Binder and D. P. Landau, Phase diagrams and critical behavior in Ising square lattices with nearest- and next-nearest-neighbor interactions, Phys. Rev. B **21**, 1941 (1980). <https://doi.org/10.1103/PhysRevB.21.1941>.
- [15] D. P. Landau, Phase transitions in the Ising square lattice with next-nearest-neighbor interactions, Phys. Rev. B **21**, 1285 (1980). <https://doi.org/10.1103/PhysRevB.21.1285>.
- [16] J. Oitmaa, The square-lattice Ising model with first and second neighbour interactions, J. Phys. A: Math. Gen. **14**, 1159 (1981). <https://doi.org/10.1088/0305-4470/14/5/03>.
- [17] D. P. Landau and K. Binder, Phase diagrams and critical behavior of Ising square lattices with nearest-, next-nearest-, and third-nearest-neighbor couplings, Phys. Rev. B **31**, 5946 (1985). <https://doi.org/10.1103/PhysRevB.31.5946>.
- [18] J. Oitmaa and M. J. Velgakis, Low-temperature series for the square lattice Ising model with first- and second-neighbour interactions. J. Phys. A: Math. Gen. **20**, 1269 (1987). <https://doi.org/10.1088/0305-4470/20/5/035>.
- [19] F. Aguilera-Granja and J. L. Morán-López, Specific heat and the phase diagram of the Ising square lattice with nearest- and next-nearest interactions, J. Phys.: Condens. Matter **5**, A195 (1993). <https://doi.org/10.1088/0953-8984/5/33A/05>.
- [20] A. Malakisa, P. Kalozoumis, and N. Tyraskis, Monte Carlo studies of the square Ising model with next-nearest-neighbor interactions, Eur. Phys. J. B **50**, 63 (2006). <https://doi.org/10.1140/epjb/e2006-00032-2>.
- [21] A. Kalz, A. Honecker, S. Fuchs, and T. Pruschke, Phase diagram of the Ising square lattice with competing interactions, Eur. Phys. J. B **65**, 533 (2008). <https://doi.org/10.1140/epjb/e2008-00359-6>.
- [22] A. Kalz, A. Honecker, S. Fuchs, and T. Pruschke, Monte Carlo studies of the Ising square lattice with competing interactions, J. Phys.: Conf. Ser. **145**, 012051 (2009). <https://doi.org/10.1088/1742-6596/145/1/012051>.
- [23] S. Jin, A. Sen, and A. W. Sandvik, Ashkin-Teller Criticality and Pseudo-First-Order Behavior in a Frustrated Ising Model on the Square Lattice, Phys. Rev. Lett. **108**, 045702, 1-5 (2012). <https://doi.org/10.1103/PhysRevLett.108.045702>.
- [24] Ansgar Kalz and Andreas Honecker, Location of the Potts-critical end point in the frustrated Ising model on the square lattice, Phys. Rev. B **86**, 134410, 1-4 (2012). <https://doi.org/10.1103/PhysRevB.86.134410>.
- [25] Songbo Jin, Arnab Sen, Wenan Guo, and Anders W. Sandvik, Phase transitions in the frustrated Ising model on the square lattice, Phys. Rev. B **87**, 144406, 1-12 (2013). <https://doi.org/10.1103/PhysRevB.87.144406>.
- [26] Yi Hu and Patrick Charbonneau, Numerical transfer matrix study of frustrated next-nearest-neighbor Ising models on square lattices, Phys. Rev. B **104**, 144429 (2021). <https://doi.org/10.1103/PhysRevB.104.144429>.
- [27] H. Li and L.-P. Yang, Tensor network simulation for the frustrated J_1 - J_2 Ising model on the square lattice, Phys. Rev. E **104**, 024118, 1-7 (2021). <https://doi.org/10.1103/PhysRevE.104.024118>.
- [28] Kota Yoshiyama and Koji Hukushima, Higher-order tensor renormalization group study of the J_1 - J_2 Ising model on a

- square lattice, Phys. Rev. E **108**, 054124 (2023). <https://doi.org/10.1103/PhysRevE.108.054124>.
- [29] Shang-Wei Li and Fu-Jiun Jiang, A Comprehensive Study of the Phase Transitions of the Frustrated J_1 - J_2 Ising Model on the Square Lattice, Prog. Theor. Exp. Phys. **2024** 053A06. <https://doi.org/10.1093/ptep/ptae061>.
- [30] Y.-H. Tseng, S.-W. Li, and F.-J. Jiang, *A comprehensive neural network study of the non-equilibrium phase transition of the two-dimensional Ising model on the square lattice*, Eur. Phys. J. Plus **139**, 776 (2024). <https://doi.org/10.1140/epjp/s13360-024-05563-8>.
- [31] <https://keras.io>; <https://www.tensorflow.org>.
- [32] Dagne Wordofa Tola and Mulugeta Bekele *Machine Learning of Nonequilibrium Phase Transition in an Ising Model on Square Lattice*, Condens. Matter **2023**, 8(3), 83. <https://doi.org/10.3390/condmat8030083>.
- [33] Metropolis, N.; Rosenbluth, A.W.; Rosenbluth, M.N.; Teller, A.H.; Teller, E. Equations of State Calculations by Fast Computing Machines. journal of Chemical Physics. 1953, **21** (6): 1087–1092. <https://doi.org/10.1063/1.1699114>.
- [34] Civitcioglu, B., Römer, R.A., Honecker, A., *Phase determination with and without deep learning*, Phys. Rev. E **111**(2), 024131 (2025). <https://doi.org/10.1103/PhysRevE.111.024131>.